Scaling of plane-wave Born cross sections for electron-impact excitation of neutral atoms

Yong-Ki Kim
National Institute of Standards and Technology, Gaithersburg, Maryland 20899-8421
(Received 12 March 2001; published 20 August 2001)

Two methods to scale plane-wave Born cross sections for electron-impact excitations of neutral atoms are shown to produce excitation cross sections comparable in accuracy to those obtained by more sophisticated collision theories such as the convergent close-coupling method. These scaling methods are applicable to integrated cross sections for electric dipole-allowed transitions. Scaled cross sections are in excellent agreement with available theoretical and experimental data for excitations in H, He, Li, Be, Na, Mg, K, Ca, Rb, Sr, Cs, Ba, Hg, and Tl, indicating the possibility of rapid and reliable calculations of excitation cross sections for many other neutral atoms.

DOI: 10.1103/PhysRevA.64.032713 PACS number(s): 34.80.Dp

I. INTRODUCTION

Two simple scaling methods for first-order, plane-wave Born cross sections for electron-impact excitations of neutral atoms are shown to produce cross sections for many neutral atoms with an accuracy comparable not only to reliable experimental data, but also to more sophisticated theories such as the *R*-matrix method [1], the convergent close coupling (CCC) [2] method, and the exterior complex scaling [3] method. The scaling methods are applicable only to dipole-allowed excitations, and use three atomic properties—the ionization energy, excitation energy, and the dipole *f* value—that can be obtained, in principle, from accurate wave functions, and hence are free of adjustable parameters. In practice, however, accurate values of the required atomic data are often available from other sources. In such cases, Born cross sections calculated from simple wave functions serve as adequate starting points, as demonstrated in this paper.

Since scaled cross sections are based on the plane-wave Born (PWB) approximation, they do not account for the resonances often found near the excitation thresholds. For applications insensitive to the details of the resonances, such as the modeling of plasma processing, plasmas in lamps, plasmas in fusion devices, and a stellar atmosphere, these scaling methods offer rapid calculation of reliable excitation cross sections for spin- and electric dipole-allowed transitions in many atoms, particularly heavy atoms and atoms with many open-shell electrons presently inaccessible to rigorous theoretical methods. The goal of the present scaling methods is to provide a simple theoretical method to calculate excitation cross sections reliable to $\pm 20\%$ or better at the cross-section peak, with an equally reliable cross-section shape for the entire range of the incident electron energy except for the region dominated by resonances. The theory is outlined in Sec. II, results are compared to available experimental and theoretical data in Sec. III, and conclusions are presented in Sec. IV.

II. THEORY

The PWB approximation is used as the starting point in the present work because (a) the plane wave is the correct wave function at infinity for an electron colliding with a neutral atom, and (b) it is the simplest collision theory that uses target wave functions explicitly. The explicit use of target wave functions enables one to use relativistic wave functions for heavy atoms, and to distinguish the final state of the target.

In a generic form, first-order PWB cross sections σ_{PWB} for inelastic collisions are written as [4]

$$\sigma_{PWB}=\frac{4\pi a_0^2 R}{T}F_{PWB}(T), \tag{1}$$

where a_0 is the Bohr radius, R is the Rydberg energy, T is the incident electron energy, and $F_{PWB}(T)$ is the collision strength (multiplied by a constant to be consistent with the standard definition of the collision strength). Qualitatively the PWB approximation does not account for the electron exchange effect with the target electrons, the distortion of plane waves in the vicinity of the target atom, or the polarization of the target due to the presence of the incident electron. The scaling methods described below combine these deficiencies into simple functional forms that depend on a few atomic properties. The proposed scaling methods apply only to integrated excitation cross sections, not to angular distributions, because the scaling methods do not alter the angular distribution shape described by the unscaled Born cross sections.

A. *BE* scaling and *C* scaling

The first scaling method, referred to as *BE* scaling, replaces the T that appears in the denominator of Eq. (1) by $T+B+E$, where B is the ionization energy, or the binding energy, of the target electron, and E is the excitation energy:

$$\sigma_{BE}=\sigma_{PWB}T/[T+B+E]. \tag{2}$$

As can be seen in the examples shown in this paper, the *BE* scaling not only reduces the cross-section magnitude at low T, but also shifts the peak to a higher T than the peak of the unscaled σ_{PWB}, while keeping the high-T validity of the PWB approximation intact.

The *BE* scaling is similar in spirit to the scaling for ionization cross sections introduced by Burgess [5,6], who used the orbital kinetic energy $U=\langle p^2\rangle/2m$ instead of E in Eq. (2). Using the Burgess scaling in combination with other approximations, Kim and Rudd [7] developed the binary-

encounter-dipole (BED) and binary-encounter-Bethe (BEB) models for electron-impact ionization cross sections. The BEB model, which is a simpler version of the BED model, uses B, U, and the orbital electron occupation number N of the ground-state orbitals of the target, and produces reliable total ionization cross sections for molecules ranging from H_2 to SF_6 at low as well as high T [8].

The original qualitative justification for the Burgess-Vrieus scaling was that the ''effective'' incident energy seen by the target electron is T plus the potential energy of the target electron. In view of the examples of the BE scaling for excitation cross sections presented here, it is clear that shifting the incident energy T in the denominator of Eq. (1) by a constant of the order of $B+E$, but not the T in the collision strength $F_{PWB}(T)$, offers a simple but effective way to account for the electron exchange, distortion, and polarization effects that are absent in the first-order PWB approximation.

At present, the BE scaling cannot be ''derived'' from first principles. In the absence of more fundamental understanding of the origin of the BE scaling, the combination $B+E$ in the BE scaling should not be taken literally as a rigid rule, but only as an indicator of the order of magnitude of a constant shift to be added to T. Indeed, the examples on some alkaline-earth elements shown later clearly indicate that a constant somewhat larger in magnitude than $B+E$ reproduces the experimental data better than using $B+E$ at intermediate and low T. Hence, as a corollary of the BE scaling, the C scaling, in which $B+E$ is replaced by a constant C, is introduced:

$$\sigma_C = \sigma_{PWB}[T/(T+C)]. \tag{3}$$

The fact that it is necessary to introduce $C>B+E$ for better agreement with experimental data for alkaline-earth elements whose resonance levels $nsnp\ ^1P$ are located above levels involving $(n-1)d$ electrons indicates that C may be related to the polarizability of the target.

A hint to the meaning of adding C to T may be found in the PWB cross section for the *elastic* scattering from the Yukawa potential. The Yukawa potential is a screened Coulomb potential,

$$V(r) = -\frac{Ze^2}{r}\exp(-r/\beta), \tag{4}$$

where r is the radial coordinate, Z is the atomic number, $-e$ is the electronic charge, and β is the ''range'' of interaction with a dimension of length. Using plane waves for the incident electron, the integrated cross section for elastic scattering is [9]

$$\sigma_{el} = 16\pi Z^2\beta^4/[a_0^2(1+4k^2\beta^2)], \tag{5}$$

where k is the momentum of the incident electron in atomic units. After writing $\beta = ba_0$ and noting that $(ka_0)^2 = T/R$, Eq. (5) becomes

$$\sigma_{el} = 4\pi a_0^2 R Z^2 b^2/(T+R/4b^2), \tag{6}$$

which has the T in the denominator shifted by a constant with the dimension of energy. Although this analogy is not rigorous, the similarity between the C scaling and Eq. (6) suggests that the constant C may be related to the shielding of the nuclear charge by the bound electrons of the target. Note that $b\to 0$ means complete screening of the nuclear charge resulting in a vanishing cross section.

A ''loose'' connection between the constant C and the electric-dipole polarizability α_d of the target atom can be demonstrated as follows. The dipole polarization potential $-e^2\alpha_d/(2r^4)$ is often introduced into the Hamiltonian of the target with some modifications to avoid the singularity at $r=0$. If the Yukawa potential is written as $V(r)\propto -[r\exp(r/\beta)]^{-1}$, then the r^{-4} term after expanding the exponential function is $-12\beta^3/r^4$. Comparison to the dipole polarization potential suggests that $\beta^3=(ba_0)^3$ plays the role of the dipole polarizability. Although this relationship is not rigorous, it implies that a study of the connection between effective screening of the nuclear charge and the polarizability of the target atom may provide a clue to the true meaning of the C scaling. Note that $C\propto b^{-2}\propto(\alpha_d)^{-2/3}$ [Eq. (6)], and $\alpha_d(\mathrm{Ca})<\alpha_d(\mathrm{Sr})<\alpha_d(\mathrm{Cs})$ according to Miller [10], which is consistent with $C(\mathrm{Ca})>C(\mathrm{Sr})>C(\mathrm{Cs})$ as listed in Table I.

B. f scaling

The PWB cross section depends on two independent approximations: (a) a first-order perturbation theory using plane waves for the incident and scattered electron, and (b) the use of approximate wave functions for nonhydrogenic targets. The BE and C scalings correct the deficiency arising from the former approximation. However, if poor target wave functions are used, the results will be unreliable regardless of the BE scaling or the C scaling, even at high T.

Although computational tools are available to generate wave functions that will produce accurate electric dipole oscillator strengths, or the f values, they are not always easy to use. In any case, the focus of the present work is not the production of extremely accurate wave functions. Fortunately, reliable experimental or theoretical f values are available for many strong transitions, and it is desirable to devise a method to take advantage of the availability of such results rather than toil to produce very accurate wave functions.

For several decades, there have been efforts to use accurate (or even not so accurate) f values to generate electron-impact excitation and ionization cross sections. Of these, perhaps the most popular one is the Gaunt-factor method [11]. In this method, the f value for the transition of interest is factored out in front of the collision strength $F_{PWB}(T)$ in Eq. (1), and then $F_{PWB}(T)$ is modified accordingly. In this way, the objective of the Gaunt-factor method is to find the appropriate collision strengths that will provide reliable cross sections.

In the BE and C scalings, the collision strength is kept intact, while the leading T is altered. The f scaling is introduced to take advantage of the availability of reliable f values from other sources. The f scaling is based on the ratio of an accurate f value to a less reliable f value produced by the

TABLE I. Resonance transition, binding energy B, excitation energy E, and scaling constant C in eV, the dipole oscillator strength f from the wave functions used for unscaled Born cross sections, and the accurate f used for the f scaling.

Atom	Transition	B	E	C	f_{Born}	f_{accurate}
H	$1s$-$2p$	13.6057	10.2043	–	0.4162	0.4162[a]
	$2s$-$3p$	13.6057	12.0940	–	0.0791	0.0791[a]
He	$1s^2$-$1s2p$ ^1P	24.5874	21.218	–	0.2671	0.2762[b]
	$1s^2$-$1s3p$ ^1P	24.5874	23.087	–	0.0730	0.0734[b]
Li	$2s$-$2p$	5.392	1.848	–	0.7683	0.7474[c]
Be	$2s^2$-$2s2p$ ^1P	9.323	5.277	–	1.341	1.373[d]
Na	$3s$-$3p$	5.139	2.104	–	1.049	0.9620[e]
Mg	$3s^2$-$3s3p$ ^1P	7.646	4.346	–	1.600	1.71[f]
K	$4s$-$4p$	4.341	1.610	–	1.222	0.9938[c]
Ca	$4s^2$-$4s4p$ ^1P	6.113	2.933	14	1.878	1.75[g]
Rb	$5s$-$5p$	4.177	1.560	–	1.330	1.023[c]
Sr	$5s^2$-$5s5p$ ^1P	5.695	2.690	12	2.036	1.84[h]
Cs	$6s$-$6p$	3.894	1.386	–	1.437	1.029[c]
Ba	$6s^2$-$6s6p$ ^1P	5.212	2.239	11	1.940	1.59[i]
Hg	$6s^2$-$6s6p$ ^1P	10.438	6.704	–	1.747	1.18[j]
Tl	$6p_{1/2}$-$6d_{3/2}$	6.108	4.478	15	0.3504	0.29[k]

[a]H. A. Bethe and E. E. Salpeter, *Quantum Mechanics of One- and Two-Electrons Atoms* (Plenum, New York, 1977), p. 265.
[b]G. W. F. Drake [18].
[c]W. R. Johnson *et al.* [19].
[d]G. Tachiev and C. F. Fischer [36].
[e]K. M. Jones *et al.* [20].
[f]P. Jönsson, C. F. Fischer, and M. R. Godefroid, J. Phys. B **32**, 1233 (1999).
[g]J. E. Hansen, C. Laughlin, H. W. van der Hart, and G. Verbockhaven, J. Phys. B **32**, 2099 (1999).
[h]Y.-K. Kim and P. S. Bagus, J. Phys. B **5**, L193 (1972).
[i]B. M. Miles and W. M. Wiese, At. Data **1**, 1 (1969).
[j]A. Lurio, Phys. Rev. **140**, A1505 (1965).
[k]A. Gallagher and A. Lurio, Phys. Rev. **136**, A87 (1964).

target wave functions being used to generate σ_{PWB}. The f scaling is given by:

$$\sigma_{PWmc} \approx (f_{mc}/f_{sc})\sigma_{PWsc}. \tag{7}$$

where σ_{PWmc} stands for the PWB cross section using accurate, or multiconfiguration wave functions with the corresponding f value denoted by f_{mc}, while σ_{PWsc} stands for the PWB cross section using uncorrelated, or single configuration wave functions with the corresponding f value denoted by f_{sc}.

The BE scaling or the C scaling and the f scaling can be applied consecutively if needed. For later use, we introduce shorthand notations

$$\sigma_{BEf} = \sigma_{BE}(f_{mc}/f_{sc}) \tag{8}$$

and

$$\sigma_{Cf} = \sigma_{C}(f_{mc}/f_{sc}). \tag{9}$$

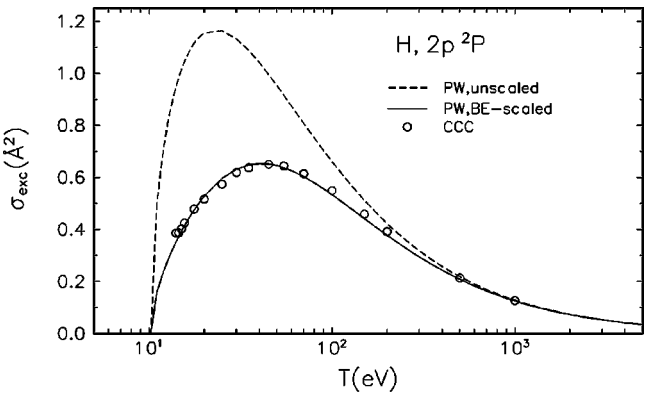

FIG. 1. Comparison of the $1s$-$2p$ excitation cross sections of H. Solid curve, plane-wave Born cross section with BE scaling; dashed curve, unscaled plane-wave Born cross section; open circles, CCC cross section [12].

C. BE scaling for electric-dipole-forbidden excitations

Application of the BE scaling to electric dipole ($E1$) forbidden transitions must be done with caution, because the PWB approximation is less successful for such transitions than for $E1$-allowed transitions. The primary reason for the poor performance of the PWB approximation for $E1$-forbidden transitions is that the PWB transition amplitude for the direct process—e.g., the $1s$-$2s$ transition in H—is small, and hence the contribution from indirect processes—e.g., $1s$-$2p$ followed by $2p$-$2s$ virtual transitions—compete with the contribution from the direct process [4].

The CCC cross sections for the $1s$-$2s$, $3s$ excitations of the hydrogen atom are lower than the corresponding PWB cross sections at intermediate T, but the former is higher than the latter near the threshold owing to the two-step virtual transitions of the type $1s$-mp followed by mp-$2s$, $3s$. Beyond the threshold region, the BE scaling described in Eq. (2) works well for the $1s$-$2s$, $3s$, and $4s$ excitations.

On the other hand, the CCC cross sections for the $1s$-$3d$, $4d$ excitations of the hydrogen atom are higher than the corresponding PWB cross sections at low and intermediate T, because the $1s$-nd excitations have substantial contributions from the second-order process of $1s$-mp followed by mp-nd virtual transitions, both steps being strong, $E1$-allowed transitions. In other words, the first-order Born approximation includes only the direct excitation from $1s$ to nd, which is weak, while the CCC method and other more complete theories would include contributions from the two-step virtual transitions described above.

III. COMPARISON TO EXPERIMENTS AND OTHER THEORIES

A. Hydrogen and helium

Unscaled PWB cross sections are compared in Figs. 1–4 to BE-scaled PWB cross sections, and the excitation cross sections from the CCC method for the $1s$-$2p$, $3p$ excitations of the hydrogen atom [12] and the $1s^2$-$1s2p$ ^1P and $1s3p$ ^1P excitations of the helium atom [13]. Figures 3 and

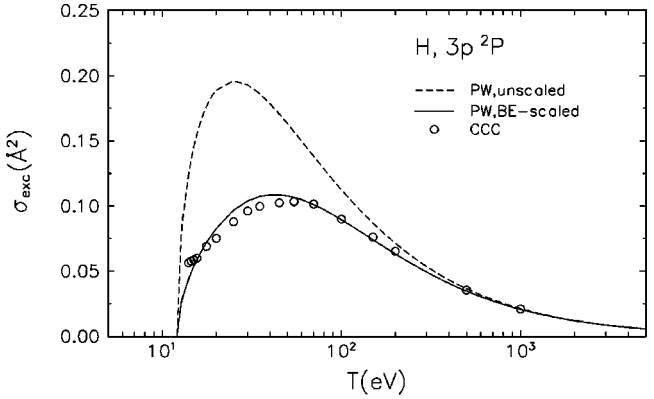

FIG. 2. Comparison of the $1s$-$3p$ excitation cross sections of H. See the caption of Fig. 1 for details.

4 for the helium atom also contain the experimental data from Westerveld *et al.* [14], the data from Shemansky *et al.* [15], the data for the $1s2p\ ^1P$ excitation recommended by Trajmar *et al.* [16], and the data of Cartwright *et al.* [17].

The data of Cartwright *et al.* for the $1s3p\ ^1P$ excitation (Fig. 4) is actually the sum of the $1s3s\ ^1S$, $1s3p\ ^1P$, and $1s3d\ ^1D$ excitation cross sections, because the excited states were too close to be separated by electron energy loss. On the other hand, Westerveld *et al.* and Shemansky *et al.* were able to isolate the ^1P transition from the others because they used emitted light to identify the excited states. The three experiments used different methods for normalization of their experimental cross sections. Westerveld *et al.* [14] normalized to the high-T values of the PWB cross section, Shemansky *et al.* [15] normalized to a dissociative excitation cross section of hydrogen, and Cartwright *et al.* [17] normalized to the elastic scattering of He at 90° and then integrated the angular distribution. Although Westerveld *et al.* cited a combined error of about 6%, the actual error limits are likely to be much higher as in the other experiments, which quote combined error limits of the order of 20%.

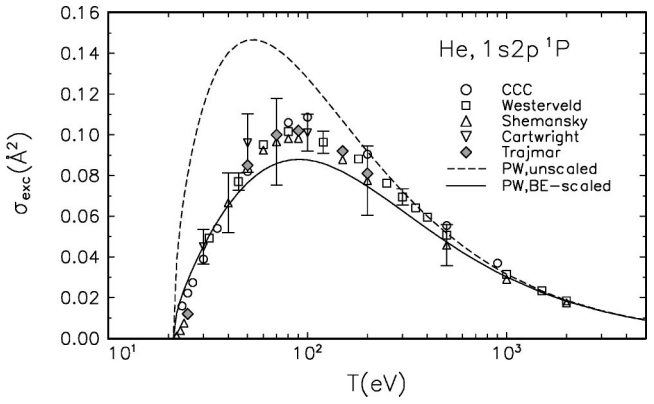

FIG. 3. Comparison of the $1s^2 \rightarrow 1s2p\ ^1P$ excitation cross sections of He. Solid curve, BE-scaled plane-wave Born cross section; dashed curve, unscaled plane-wave Born cross section; circles, CCC cross section [13]; squares, experimental data of Westerveld *et al.* [14]; upright triangles, data of Shemansky *et al.* [15]; inverted triangles, data of Cartwright *et al.* [17]; diamonds, cross section recommended by Trajmar *et al.* [16].

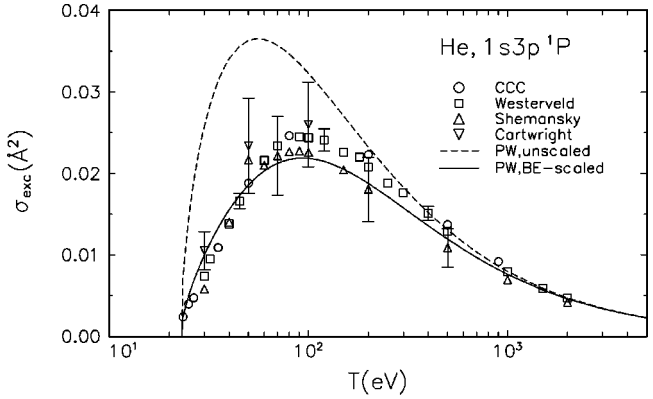

FIG. 4. Comparison of the $1s^2$-$1s3p\ ^1P$ excitation cross sections of He. See the caption of Fig. 3 for details.

Except for the presence of resonances near the thresholds in the CCC cross sections, the performance of the *BE*-scaled PWB cross sections is remarkable, particularly in view of the simplicity of the scaling. The agreement of the *BE*-scaled PWB cross sections with the CCC cross sections for He is not as good as for the hydrogen atom. However, the CCC cross sections for He are not as accurate as those for H because of the approximate nature of the CCC wave functions. Although not included in the present paper, the agreement between the *BE*-scaled PWB cross sections with the CCC cross sections and available experimental data for the $1s$-$4p$ excitation of H and $1s^2$-$1s4p\ ^1P$ excitation of He is as good as those shown in Figs. 1–4.

Independent of the choice of collision theory, the accuracy of wave functions becomes an issue for multielectron atoms. As is shown in Table I, the uncorrelated Dirac-Fock wave functions used for He in the present work produce f values of 0.2671 and 0.0730 for the $1s2p\ ^1P$ and $1s3p\ ^1P$ excitations, respectively, to be compared to the accurate values of 0.2762 and 0.0734 [18]. To obtain cross sections of modest accuracy, the uncorrelated wave functions used in Figs. 3 and 4 are sufficient.

B. Alkali metals

For alkali metals, the *BE* and *f*-scaled PWB cross sections for the resonance excitations, ns-np, are in excellent agreement with available experimental and ''reliable'' theoretical cross sections. For alkali metals, uncorrelated Dirac-Fock wave functions were used to calculate unscaled Born cross sections. More accurate f values used for the f scaling of alkali metals are from the relativistic random-phase approximation results calculated by Johnson *et al.* [19]. For Na, we used the f value deduced from trapped atoms [20].

The most reliable experimental excitation cross sections for the resonance transitions of alkali metals are those from the optical emission of alkali atoms after excitation by electron impact. From the wavelength of the emitted light, the transition is positively identified. On the other hand, the optical emission data in general contain cascades from higher levels. The correction for cascades requires the knowledge of excitation cross sections to all higher levels that feed into the

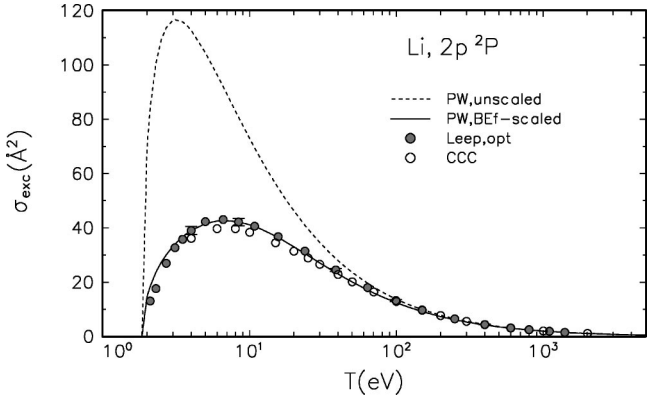

FIG. 5. Comparison of the $2s$-$2p$ excitation cross sections of Li. Dashed curve, unscaled σ_{PWB}; solid curve, *BE*- and *f*-scaled σ_{PWB}; triangles, experimental data for optical emission from Leep and Gallagher [21]; circles, CCC theory of Schweinzer *et al.* [29].

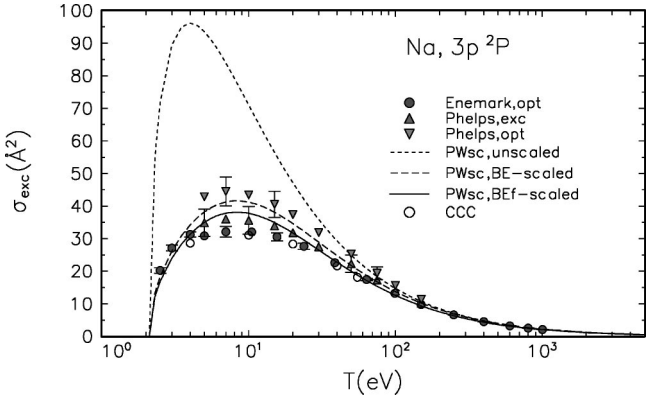

FIG. 6. Comparison of the $3s$-$3p$ excitation cross sections of Na. Filled circles: experimental data of Enemark and Gallagher [22]; triangles: data of Phelps and Lin [30]; solid curve: PWB cross section from uncorrelated wave functions after *BE* and *f* scaling; short-dashed curve: unscaled PWB cross section; medium-dashed curve: PWB cross section after *BE* scaling; open circles: CCC cross section [31].

excited level of interest and the transition probabilities between the feeding levels and the excited level of interest. In addition, the emission cross section as a function of the incident energy is often measured relatively, and then the absolute scale is fixed by comparison to other cross sections for which absolute scale is known.

Almost three decades ago, Gallagher and co-workers used the optical emission method to measure electron-impact excitation cross sections for the resonance transitions of Li [21], Na [22], Mg [23], K [24], Ca [25], Rb [24], Sr [26], Cs [24], Ba [27], and Tl [28]. Their relative cross sections were normalized to the PWB cross sections at the value of high T available then. When experimental f values more accurate than implied by the Born cross sections were available, Gallagher and co-workers replaced the theoretical f-value in the leading high-T term of the Born cross section, known as the Bethe cross section, by the experimental one, but kept the rest of the atomic parameters in the Bethe cross section unchanged. This is slightly different from the f scaling described in Sec. II B. The latter scales the entire Born cross section by the ratio of the f values, while the former scales only part of the Born cross section.

In Figs. 5–9, the scaled PWB cross sections are compared to experimental data for the resonance transitions of Li, Na, K, Rb, and Cs, respectively. Figure 5 also contains the CCC cross section of Schweinzer *et al.* [29], which is in excellent agreement with the experiment by Leep and Gallagher [21]. The scaled Born cross section shown in Fig. 5 used only *BE* scaling to demonstrate that the *BE*-scaled cross section from uncorrelated wave functions is adequate when the difference between the uncorrelated and correlated f values (Table I) is small.

In Fig. 6, unscaled, *BE*-scaled, and f-scaled PWB cross sections for the $3s$-$3p$ excitation of Na are compared to the experimental data of Enemark and Gallagher [22], the data of Phelps and Lin [30], and the CCC cross section of Bray [31]. The f value from the uncorrelated Dirac-Fock wave functions—actually sum of the excitations to the $3p_{1/2}$ and $3p_{3/2}$ levels—is 1.049 while the most accurate value is 0.9620 [20]. Hence the f scaling reduces the *BE*-scaled cross section further by about 10%. Figure 6 includes the first example of applying both the *BE* and f scalings to the PWB excitation cross section from uncorrelated wave functions. The scaled cross section for K is compared in Fig. 7 to the experimental data of Chen and Gallagher [24], those of Phelps *et al.* [32], and theoretical cross sections calculated by Phelps *et al.* [32] using the close-coupling theory with 15 states. The largest source of experimental uncertainty in the emission cross sections measured by Gallagher *et al.* is in the normalization of relative cross sections to the asymptotic Born cross sections. The normalization uncertainty ranges from 3% to 6%, while the uncertainties associated with the relative cross sections are typically 1% or less. The direct excitation cross section by definition is lower than the emission cross section, because the latter contains contributions from cascades. If excitation cross sections and decay rates for all upper levels contributing to the cascade are known,

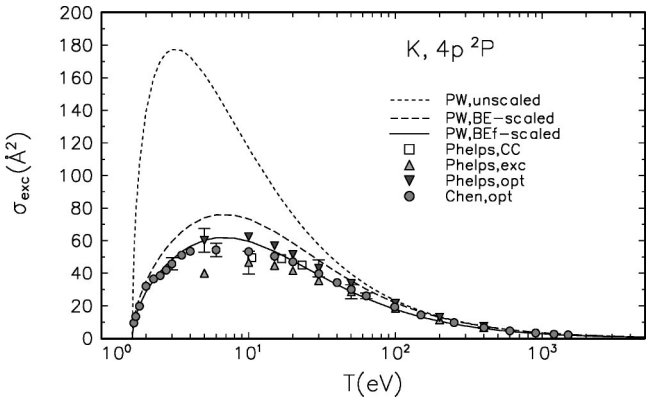

FIG. 7. Comparison of the $4s$-$4p$ excitation cross sections of K. Short-dashed curve: unscaled σ_{PWB}; medium-dashed curve: *BE*-scaled σ_{PWB}; solid curve: *BE*- and *f*-scaled σ_{PWB}; squares: 15-state close-coupling theory of Phelps *et al.* [32]; upright triangles: experimental data for direct excitation by Phelps *et al.* [32]; inverted triangles: data for optical emission from Phelps *et al.* [32]; circles: data for optical emission from Chen and Gallagher [24].

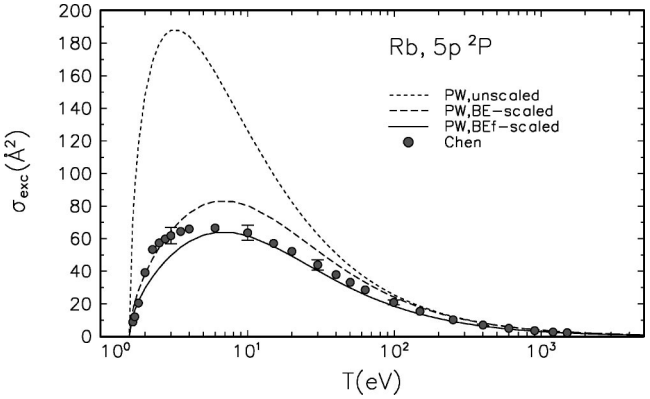

FIG. 8. Comparison of the $5s$-$5p$ excitation cross sections of Rb. Short-dashed curve, unscaled σ_{PWB}; medium-dashed curve, BE-scaled σ_{PWB}; solid curve, BE- and f-scaled σ_{PWB}; circles, experimental data for optical emission from Chen and Gallagher [24].

then theory can reconstruct the emission cross section that can be compared to the experiment.

Conversely, cascades to the lowest resonance lines can often be estimated and subtracted from the emission cross section. The resulting direct excitation cross sections can be compared to theoretical excitation cross sections, including the present scaled PWB cross sections. The estimated cascade contribution for the $3s$-$3p$ transition of Na (Fig. 6) near the cross section peak is approximately 10% according to Phelps and Lin [30], while the cascade contribution for the $4s$-$4p$ transition of K (Fig. 7) near the peak is approximately 25% [32].

A slight bulge in the experimental data at $T=2-3$ eV in Rb (Fig. 8) and Cs (Fig. 9) is likely to have resulted from cascades or constructive interference with nearby levels. These secondary effects are not included in the PWB approximation.

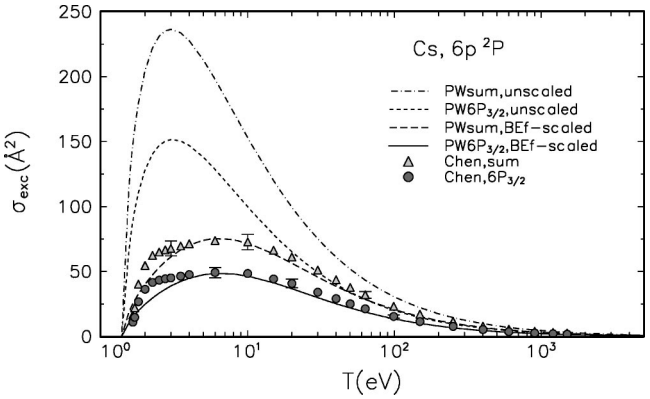

FIG. 9. Comparison of the $6s$-$6p$ excitation cross sections of Cs. Dot-dashed curve, unscaled σ_{PWB} for the $6s$-$6p_{1/2}+6p_{3/2}$ excitations; short-dashed curve, unscaled σ_{PWB} for the $6s$-$6p_{3/2}$ excitation; medium-dashed curve, BE- and f-scaled σ_{PWB} for the $6s$-$6p_{1/2}+6p_{3/2}$ excitations; solid curve, BE- and f-scaled σ_{PWB} for the $6s$-$6p_{3/2}$ excitation; triangles, experimental data for the $6s$-$6p_{1/2}+6p_{3/2}$ excitations from Cheng and Gallagher [24]; circles, data for the $6s$-$6p_{3/2}$ excitation from Cheng and Gallagher [24].

TABLE II. Scaled Born cross sections in Å^2 for the resonance transitions of alkali metals and Hg. T is the incident electron energy in eV; σ_{BEf} is the BE- and f-scaled cross section [Eq. (8)].

	σ_{BEf}					
T	Li	Na	K	Rb	Cs($6p_{3/2}$)	Hg
2	14.61		28.52	29.47	24.89	
3	33.18	24.01	48.34	49.60	38.86	
4	39.01	31.36	56.50	58.17	44.88	
5	41.51	35.02	60.20	62.11	47.54	
6	42.49	36.91	61.68	63.71	48.52	
8	42.37	38.12	61.50	63.62	48.11	1.20
10	41.11	37.77	59.61	61.69	46.44	2.03
15	36.91	34.92	53.34	55.23	41.30	3.12
20	33.01	31.74	47.59	49.29	36.71	3.57
25	29.76	28.92	42.83	44.37	32.95	3.74
30	27.08	26.52	38.93	40.33	29.90	3.78
40	22.98	22.75	32.99	34.18	25.28	3.69
50	20.01	19.95	28.70	29.75	21.97	3.52
60	17.75	17.79	25.47	26.40	19.48	3.33
80	14.56	14.70	20.89	21.66	15.96	2.98
100	12.40	12.59	17.79	18.46	13.59	2.69
150	9.14	9.36	13.14	13.64	10.03	2.16
200	7.30	7.51	10.51	10.91	8.02	1.82
300	5.28	5.46	7.61	7.91	5.81	1.39
400	4.17	4.33	6.02	6.26	4.60	1.14
500	3.46	3.61	5.01	5.21	3.82	0.967
600	2.97	3.11	4.30	4.48	3.29	0.844
800	2.33	2.45	3.38	3.52	2.58	0.678
1000	1.93	2.03	2.80	2.91	2.14	0.570
2000	1.06	1.12	1.55	1.61	1.18	0.328

For Cs (Fig. 9), Chen and Gallagher [24] actually measured the $6s$-$6p_{3/2}$ transition, because the fine-structure splitting between the $6p_{1/2}$ and $6p_{3/2}$ levels is large. However they published the sum of the excitations to the two levels by multiplying the measured cross section by 1.5. Since Dirac-Fock wave functions were used in the present work, the Born excitation cross sections to the two $6p$ levels were calculated separately, and are included in Fig. 9.

Comparisons to other theories, such as close coupling, can be found in earlier papers reporting experimental results on the resonance transitions of alkali metals, e.g., by Williams *et al.* [33] and Vušković *et al.* [34] for Li. These are electron-energy-loss measurements which lead to direct excitation cross sections free of cascades. However, they measure angular distributions at each incident energy, and usually have larger uncertainties than optical emission results due to the extrapolation over forward and backward angles not covered by experiment. Scaled Born cross sections for the alkali metals are listed in Table II.

C. Alkaline-earth elements

The scaled Born cross sections are compared to other experimental and theoretical data for the resonance transitions of Be, Mg, Ca, Sr, and Ba in Figs. 10–14, respectively. Mul-

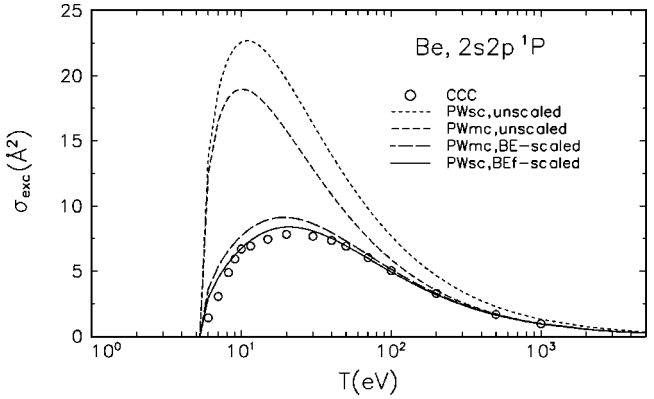

FIG. 10. Comparison of the $2s^2$-$2s2p\ ^1P$ excitation cross sections of Be. Circles, CCC cross section [36]; short-dashed curve, unscaled plane-wave Born cross section from uncorrelated wave functions; medium-dashed curve, unscaled plane-wave Born cross section from multiconfiguration wave functions; long-dashed curve, *BE*-scaled plane-wave Born cross section from multiconfiguration wave functions; solid curve, *BE* and *f*-scaled plane-wave Born cross section from uncorrelated wave functions.

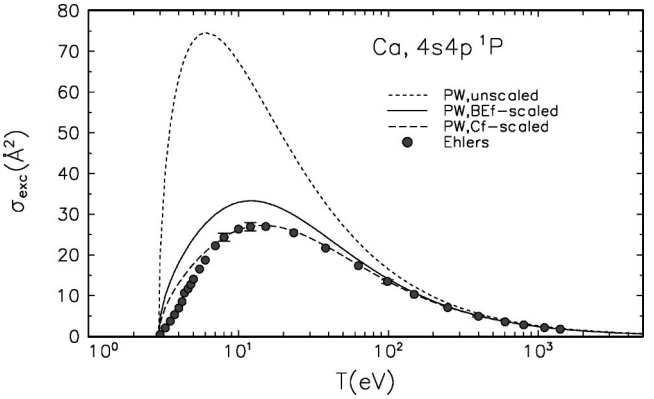

FIG. 12. Comparison of the $4s^2$-$4s4p\ ^1P$ excitation cross sections of Ca. Short-dashed curve, unscaled σ_{PWB}; solid curve, *BE*- and *f*-scaled σ_{PWB}; medium-dashed curve, *C*- and *f*-scaled σ_{PWB}; circles, experimental data for optical emission from Ehlers and Gallagher [25].

ticonfiguration Dirac-Fock wave functions—relativistic equivalents of $ns^2+np^2+n'd^2$ for the ground state and $nsnp+npn'd$ for the ^1P state, where n' is either $n-1$ or n—were used to calculate unscaled PWB cross sections for these alkaline-earth elements.

Unlike the case of alkali metals, it was necessary to use the *C* and *f* scalings for the resonance excitations of heavier alkaline-earth elements Ca, Sr, and Ba, while *BE* and *f* scalings led to excellent agreement with experiments on Be and Mg. The values of *B*, *E*, *C*, and *f* used in scaling the PWB cross sections are listed in Table I.

For Be, uncorrelated Dirac-Fock wave functions (labeled PW*sc* in Fig. 10) produce an *f* value of 1.864 compared to an accurate value of 1.373 [35]. The PWB excitation cross sections for the $2s^2$–$2s2p\ ^1P$ transition of Be is compared in Fig. 10 to the cross section calculated by the CCC method [36]. The correlated, multiconfiguration wave functions used for the PWB cross section—$2s^2+2p^2+3d^2$ for the ground state and $2s2p+2p3d$ for the excited state, labeled as PW*mc* in Fig. 10—lead to an *f* value of 1.341 compared to the CCC value of 1.386. Figure 10 indicates that *BE*-scaled PWB cross sections calculated from wave functions of modest accuracy with only a few extra configurations reproduce the CCC cross section well.

Although Figs. 3–5 clearly demonstrate the utility of the *BE* scaling applied to PWB cross sections calculated from wave functions of limited accuracy, note that the transitions shown are all strong, *E*1-allowed transitions. Occasionally, unexpected cancellations in the *E*1 transition matrix elements—often referred to as the Cooper minimum if the cancellation occurs in the continuum—result in very small *f* values. The $2s^2$-$2s3p\ ^1P$ excitation of neutral Be is such a case. Unlike the case of the $2s2p\ ^1P$ excitation of Be, uncorrelated Dirac-Fock wave functions for the $2s3p\ ^1P$ excitation lead to an *f* value of 0.2131, while the correct value is 0.0080 [36] due to heavy cancellations in the transition matrix element. In such cases, secondary effects, such as the

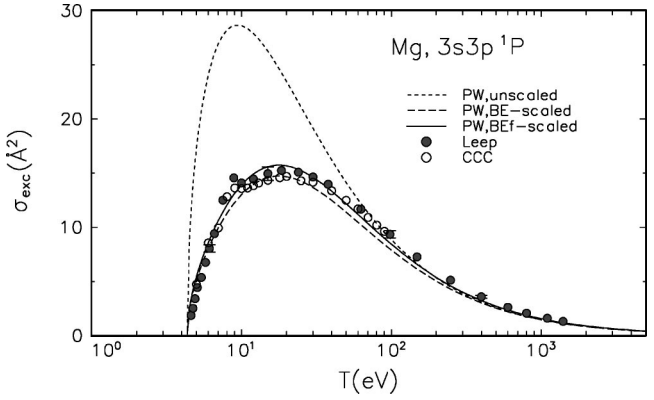

FIG. 11. Comparison of the $3s^2$-$3s3p\ ^1P$ excitation cross sections of Mg. Short-dashed curve, unscaled σ_{PWB}; medium-dashed curve, *BE*-scaled σ_{PWB}; solid curve, *BE*- and *f*-scaled σ_{PWB}; circles, experimental data for optical emission from Leep and Gallagher [23]; circles: CCC theory [37].

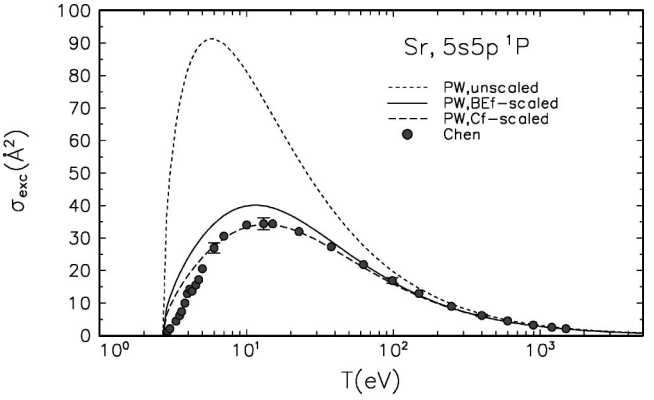

FIG. 13. Comparison of the $5s^2$-$5s5p\ ^1P$ excitation cross sections of Sr. Short-dashed curve, unscaled σ_{PWB}; solid curve, *BE*- and *f*-scaled σ_{PWB}; medium-dashed curve, *C*- and *f*-scaled σ_{PWB}; circles, experimental data for optical emission from Chen *et al.* [26].

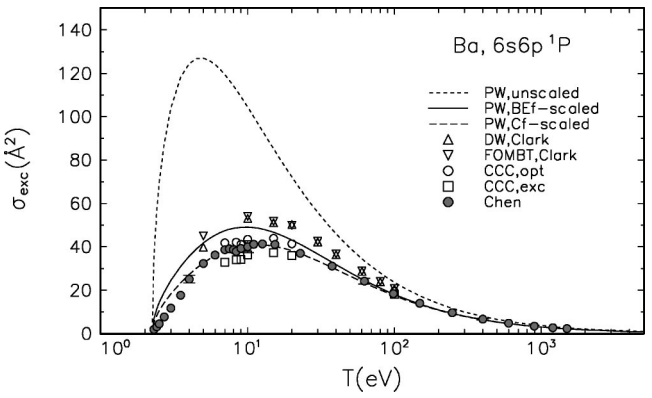

FIG. 14. Comparison of the $6s^2$-$6s6p$ ^1P excitation cross sections of Ba. Short-dashed curve, unscaled σ_{PWB}; solid curve, *BE*- and *f*-scaled σ_{PWB}; medium-dashed curve, *C*- and *f*-scaled σ_{PWB}; upright triangles, distorted-wave Born theory of Clark *et al.* [39]; inverted triangles, first-order many-body theory of Clark *et al.* [39]; open circles, CCC theory for optical emission; squares, CCC theory for direct excitation; filled circles, experimental data for optical emission from Chen and Gallagher [27].

two-step virtual excitations described earlier, dominate while the PWB approximation is incapable of representing such effects.

The CCC cross sections for Mg [37] and Ba [38] are included for comparison in Figs. 11 and 14, respectively. For Ba in Fig. 14, theoretical results based on the distorted-wave Born approximation and the first-order many-body theory by Clark *et al.* [39] are also included. Figure 14 clearly demonstrates the utility of the present work, even without *C* scaling, compared to theories other than the CCC method. Fursa and Bray [38] reported that the cascade contribution near the peak of the Ba cross section is approximately 20%, similar to the estimate by Phelps *et al.* [32] for K.

For Be and Mg, the *BE* scaling was sufficient to convert PWB cross sections into excellent agreement with available experimental data. However, as Figs. 12–14 demonstrate, the *C* scaling improves the agreement between scaled Born cross sections and experiments for heavier alkaline-earth elements. The values of *C* required for Ca, Sr, and Ba are 4–5 eV higher than $B+E$, as can be seen from Table I. The experimental data for Ca, Sr, and Ba near the thresholds are lower than the scaled Born cross sections, while an opposite trend is seen in Rb and Cs. This may be an indication of destructive interference with nearby levels. Scaled Born cross sections for the alkaline-earth elements are listed in Table III.

D. Mercury and thallium

Applications of the *BE* and the *f* scalings were successful in reproducing the experimental data on the resonance transition of Hg [40,41], while *C* and *f* scalings produced a slightly better agreement with experiment for the $6p_{1/2}$-$6d_{3/2}$ excitation of Tl [28]. Note that the Tl excitation is a p-d transition unlike the examples presented so far.

In Fig. 15 the present scaled PWB cross sections are compared to experimental data [40,41] for the resonance transition $6s^2$-$6s6p$ ^1P of Hg, as well as to the relativistic distorted-wave Born cross section of Srivastava *et al.* [42]. Again, the present scaled Born cross section is in much better agreement with the experiments.

TABLE III. Scaled Born cross sections in Å^2 for the resonance transitions of alkaline-earth elements and Tl. *T* is the incident electron energy in eV; σ_{BEf} is the *BE*- and *f*-scaled cross section [Eq. (8)]; σ_{Cf} is the *C*- and *f*-scaled equation cross section [Eq. (9)].

	σ_{BEf}		σ_{Cf}			
T	Be	Mg	Ca	Sr	Ba	Tl
3			3.29	8.94	18.26	
4			13.11	18.55	27.21	
5		5.41	17.76	23.97	32.52	0.196
6	2.96	8.57	20.80	27.50	35.88	0.430
8	5.48	12.06	24.36	31.51	39.44	0.784
10	6.76	13.90	26.13	33.34	40.76	1.03
15	8.09	15.58	27.24	34.04	40.31	1.35
20	8.38	15.66	26.60	32.80	38.17	1.47
25	8.30	15.22	25.45	31.09	35.77	1.51
30	8.65	14.61	24.18	29.34	33.48	1.50
40	7.51	13.33	21.80	26.19	29.55	1.44
50	6.94	12.17	19.75	23.58	26.41	1.36
60	6.43	11.17	18.05	21.44	23.88	1.28
80	5.59	9.60	15.40	18.18	20.10	1.13
100	4.94	8.43	13.46	15.82	17.41	1.02
150	3.86	6.52	10.32	12.06	13.18	0.811
200	3.19	5.35	8.43	9.82	10.69	0.678
300	2.40	3.99	6.25	7.26	7.86	0.517
400	1.94	3.22	5.01	5.81	6.27	0.422
500	1.63	2.71	4.21	4.87	5.25	0.358
600	1.42	2.35	3.64	4.21	4.53	0.312
800	1.13	1.87	2.88	3.33	3.58	0.251
1000	0.946	1.56	2.40	2.77	2.97	0.211
2000	0.536	0.881	1.35	1.55	1.66	0.121

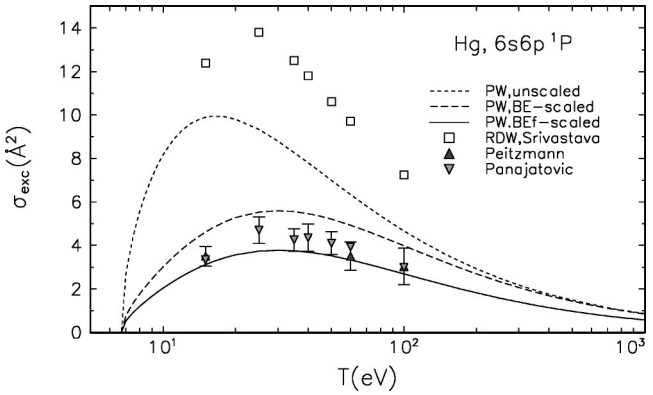

FIG. 15. Comparison of the $6s^2$-$6s6p$ ^1P excitation cross sections of Hg. Short-dashed curve, unscaled σ_{PWB}; medium-dashed curve, *BE*-scaled σ_{PWB}; solid curve, *BE*- and *f*-scaled σ_{PWB}; squares, relativistic distorted-wave Born theory of Srivastava *et al.* [42]; upright triangles, experimental data for direct excitation from Peitzmann and Kessler [40]; inverted triangles, data for direct excitation from Panajatović *et al.* [41].

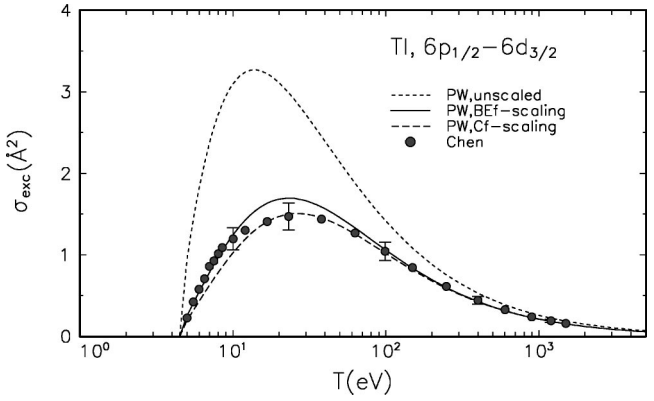

FIG. 16. Comparison of the $6p_{1/2}$-$6d_{3/2}$ excitation cross sections of Tl. Short-dashed curve, unscaled σ_{PWB}; *BE*- and *f*-scaled σ_{PWB}; medium-dashed curve, *C*- and *f*-scaled σ_{PWB}; circles, experimental data for optical emission from Chen and Gallagher [28].

In Fig. 16 the present scaled PWB cross sections for the $6p_{1/2}$-$6d_{3/2}$ excitation of Tl are compared to the experimental result by Chen and Gallagher [28]. The scaled Born cross section for Hg is listed in Table II, and the scaled Born cross section for Tl in Table III.

In the same paper, Chen and Gallagher [28] also reported cross sections for the $6p_{1/2}$-$7s$ and $6p_{1/2}$-$6d_{5/2}$ excitations of Tl. According to the authors, the optical emission from the $7s$ level is strongly affected by cascades from higher levels, while the emission from the $6d_{3/2}$ level is not. Their excitation cross section to the $7s$ level is about 20% higher than the scaled PWB cross sections at $T=20$ eV, consistent with an uncertainty of 6% from normalization and 16% from cascade estimated by the authors. However, their $6d_{5/2}$ excitation cross section is almost double the scaled Born cross sections at the peak, though there is clear similarity in the cross section shape typical of a dipole-forbidden excitation. The authors estimated their uncertainty for the $6d_{5/2}$ excitation cross section to be $\pm 16\%$ from normalization and $\pm 1\%$ from cascades.

IV. CONCLUSIONS

After comparing the similarities in shape and magnitude of the resonance excitation cross sections of alkaline-earth elements, Chen and Gallagher [27] voiced their hope that ''these comparisons will help stimulate a search for a simple universal improvement on the Born and Bethe approximations for this intermediate-energy range.'' The scalings described in the present work come close to fulfilling their wish, though belatedly. Indeed, all the cross sections for the alkali metals in Table II peak around $T=6$ eV, although the peak values form three groups, Li and Na on the low side, K and Rb on the high side, and Cs in between. The Cs peak value is a surprise because it is the largest atom in the Periodic Table. The cross sections for the alkaline-earth elements in Table III are less uniform, though they all peak between $T=15$ and 20 eV.

The results presented in this paper demonstrate the utility of the concept of adding a constant to the incident electron energy T in the denominator of Eq. (1) as a simple way to obtain reliable electron-impact cross sections for dipole-allowed excitations of neutral atoms. The *BE* and *C* scalings not only change the peak value, but also the cross-section shape at low incident energies. On the other hand, the *f* scaling changes only the magnitude but not the shape. The effectiveness of the simple *BE* scaling is too universal to be an accident, and it would be good if a rigorous theoretical justification for these scalings can be found soon.

The *C* scaling cannot be used to predict unknown cross sections at present, because there is no recipe to determine the value of *C* for such cases. However, the *BE* and *f* scalings can be used to predict cross sections, because the values of *B* and *E* are either available in the literature, or can be calculated from high-quality wave functions, which can also be used to calculate the required PWB cross sections and *f* values. The examples of Ca, Sr, Ba, and Tl (Figs. 12–14, and 16) indicate that BE- and *f*-scaled cross sections may be in error by 20% or less at the peak, still much better than using unscaled PWB cross sections, or other theories based on the first-order perturbation, as demonstrated in Fig. 14. From the examples presented here, the *C* scaling seems to be required if the upper level of the resonance transition is not the first excited state. However, the *C* scaling was unnecessary for the $1s$-$3p$ excitation of H and the $1s^2$-$1s3p$ ^1P excitation of He. Note that the values of *C* are close to 1.5 times the values of $B+E$ for Ca, Sr, Ba, and Tl (Table I).

It is pointed out that the *elastic* scattering cross section of an electron scattered by the Yukawa potential has a form similar to the *C* scaling [Eq. (3)], hinting at the possibility that the constant *C* is related to the screening of the nuclear charge. Also, a ''loose'' inverse dependence of *C* on the dipole polarizability α_d is demonstrated. These relations, however, do not constitute a proof or derivation of *BE* and *C* scalings. The true origin of the scalings still remains a mystery.

The essence of the *BE* scaling and the Burgess scaling is adding a constant to the T in the denominator of Eq. (1). This T in conventional collision theory is introduced to normalize the flux of incident electrons, i.e., the number of incident electrons passing through a unit area perpendicular to the incident electron path in unit time. Adding a constant to T then can be interpreted as increasing the effective flux of incident electrons, or ''focusing'' of the incident electrons. Indeed, the Burgess scaling is often called the focusing correction in the binary encounter theory [6].

The success of the *BE* and *f* scalings shown in this paper should not diminish the value of more sophisticated methods that produce highly accurate results [1–3], though they require orders of magnitude more computational effort than PWB cross sections. First of all, rigorous and reliable results are needed to confirm that the *BE* scaling is reliable and safe to use. Second, the *BE* scaling will not work well on angular distributions because the scaling only changes the T dependence of PWB cross sections. It is well known that PWB cross sections do not reproduce large angle scattering well at any T, and the *BE* scaling will not change the shape of PWB angular distributions.

The scalings described here will facilitate the calculation of integrated excitation cross sections for many neutral at-

oms, particularly for atoms with open valence orbitals, which pose difficulties to more computer-intensive theories. Moreover, the f scaling permits the use of simple wave functions as long as accurate f values are available through other means, as was done for heavy atoms in this article.

The present scalings should also work, with minor adjustments if needed, on ions using the Coulomb Born cross sections as the starting point. Indeed, preliminary results for the excitations of singly-charged atomic ions indicate that C in Eq. (3) should be of the order of E without B. Work on scaled Coulomb Born cross sections for atomic ions is in progress.

Application of the present BE and f scalings to the ns^2np-$nsnp^2$ transitions in Al, Ga, and In leads to excellent agreement between theory and experiments on the total ionization cross sections, which consist of almost equal contributions from the direct ionization and the excitation-autoionization of the ns excited levels [43].

Finally, applicability of the present scalings to molecular excitation cross sections should be a worthwhile topic to study. In view of the success of the BEB model for molecular ionization cross sections [7], it is almost certain that scalings similar to those presented here should be effective for dipole-allowed molecular excitations.

ACKNOWLEDGMENTS

This work was partly supported by the Office of Fusion Sciences of the U.S. Department of Energy and by NIST's Advanced Technology Program. The author is grateful for many illuminating discussions with Dr. P. Stone.

[1] P. Burke and K. Berrington, *Atomic and Molecular Processes: An R-Matrix Approach* (Institute of Physics Publishing, Bristol, 1993).
[2] I. Bray and A. T. Stelbovics, Adv. At. Mol. Phys. **35**, 290 (1995).
[3] M. Baertschy, T. N. Resigno, W. A. Issacs, X. Li, and C. W. McCurdy, Phys. Rev. A **63**, 022712 (2001).
[4] M. Inokuti, Rev. Mod. Phys. **43**, 297 (1971).
[5] A. Burgess, in *Proceedings of the Third International Conference on Electronic and Atomic Collisions, London, 1963*, edited by M. R. C. McDowell (North-Holland, Amsterdam, 1964), p. 237; Proceedings of the Symposium on Atomic Collision Processes in Plasmas, Culham, 1964 (AERE Report No. 4818), p. 63.
[6] L. Vriens, in *Case Studies in Atomic Physics*, edited by E. W. McDaniel and M. R. C. McDowell (North-Holland, Amsterdam, 1969), Vol. 1, p. 335.
[7] Y.-K. Kim and M. E. Rudd, Phys. Rev. A **50**, 3954 (1994).
[8] References and ionization cross sections for H, He, and many molecules are available from http://physics.nist.gov/ionxsec.
[9] For instance, see C. J. Joachain, *Quantum Collision Theory* (North-Holland, Amsterdam, 1975), p. 175, Eq. (8.92).
[10] T. M. Miller, *CRC Handbook of Chemistry and Physics*, edited by D. R. Lide, 77th ed. (CRC Press, New York, 1996), p. **10**-199.
[11] S. M. Younger and W. L. Wiese, J. Quant. Spectrosc. Radiat. Transf. **22**, 161 (1979).
[12] I. Bray and A. T. Stelbovics, Phys. Rev. A **46**, 6995 (1992).
[13] D. V. Fursa and I. Bray, Phys. Rev. A **52**, 1279 (1995).
[14] W. B. Westerveld, H. G. Heideman, and J. van Eck, J. Phys. B **12**, 115 (1979).
[15] D. E. Shemansky, J. M. Ajello, D. T. Hall, and B. Franklin, Astrophys. J. **296**, 774 (1985).
[16] S. Trajmar, J. M. Ratliff, G. Csanak, and C. C. Cartwright, Z. Phys. D: At., Mol. Clusters **22**, 457 (1992).
[17] D. C. Cartwright, G. Csanak, S. Trajmar, and D. F. Register, Phys. Rev. A **45**, 1602 (1992).
[18] G. W. F. Drake in *Atomic, Molecular, and Optical Physics Handbook*, edited by G. W. F. Drake (AIP, Woodbury, NY, 1996), Chap. 11.
[19] W. R. Johnson, Z. W. Liu, and J. Sapirstein, At. Data Nucl. Data Tables **64**, 279 (1996).
[20] K. M. Jones, P. S. Julienne, P. D. Lett, W. D. Phillips, E. Tiesinga, and C. J. Williams, Europhys. Lett. **35**, 85 (1996).
[21] D. Leep and A. Gallagher, Phys. Rev. A **10**, 1082 (1974).
[22] E. A. Enemark and A. Gallagher, Phys. Rev. A **6**, 192 (1972).
[23] D. Leep and A. Gallagher, Phys. Rev. A **13**, 148 (1976).
[24] S. T. Chen and A. C. Gallagher, Phys. Rev. A **17**, 551 (1978).
[25] V. J. Ehlers and A. Gallagher, Phys. Rev. A **7**, 1573 (1973).
[26] S. T. Chen, D. Leep, and A. Gallagher, Phys. Rev. A **13**, 947 (1976).
[27] S. T. Chen and A. Gallagher, Phys. Rev. A **14**, 593 (1976).
[28] S. T. Chen and A. Gallagher, Phys. Rev. A **15**, 888 (1977).
[29] J. Schweinzer, R. Brandenburg, I. Bray, R. Hoekstra, F. Aumayr, R. K. Janev, and H. P. Winter, At. Data **72**, 239 (1999).
[30] J. O. Phelps and C. C. Lin, Phys. Rev. A **24**, 1299 (1981).
[31] I. Bray, Phys. Rev. A **49**, 1066 (1994).
[32] J. O. Phelps, J. E. Solomon, D. F. Korff, and C. C. Lin, Phys. Rev. A **20**, 1418 (1979).
[33] W. Williams, S. Trajmar, and D. Bozinis, J. Phys. B **9**, 1529 (1976).
[34] L. Vušković, S. Trajmar, and D. F. Register, J. Phys. B **15**, 2517 (1982).
[35] G. Tachiev and C. F. Fischer, J. Phys. B **32**, 5805 (1999).
[36] D. V. Fursa and I. Bray, J. Phys. B **30**, 5895 (1997).
[37] D. V. Fursa and I. Bray, Phys. Rev. A **63**, 032708 (2001).
[38] D. V. Fursa and I. Bray, Phys. Rev. A **59**, 282 (1999).
[39] R. E. H. Clark, J. Abdallah, Jr., G. Csanak, and S. P. Kramer, Phys. Rev. A **40**, 2935 (1989).
[40] F. J. Peitzmann and J. Kessler, J. Phys. B **23**, 2629 (1990).
[41] R. Panajatović, V. Pejčev, M. Konstantinović, D. Filipović, V. Bočvarski, and B. Marinković, J. Phys. B **26**, 1005 (1993).
[42] R. Srivastava, T. Zuo, R. P. McEachran, and A. D. Stouffer, J. Phys. B **26**, 1025 (1993).
[43] Y.-K. Kim and P. M. Stone, Phys. Rev. A (to be published).